HHS Public Access

Author manuscript

J Magn Reson Imaging. Author manuscript; available in PMC 2024 September 01.

Published in final edited form as:

J Magn Reson Imaging. 2023 September ; 58(3): 807–814. doi:10.1002/jmri.28572.

Cine MRI-derived radiomics features of the cardiac blood pool: Periodicity, Specificity, and Reproducibility

Kai Lin, MD, MS,

Roberto Sarnari, MD,

James C. Carr, MD,

Michael Markl, PhD

Department of Radiology, Northwestern University, 737 N Michigan Avenue, Suite 1600, Chicago, IL 60611

Abstract

Background—Although radiomics features of the left ventricular wall has been used to assess cardiac diseases, radiomics features of the cardiac blood pool have been relatively ignored.

Purpose—To test the hypothesis that cine MRI-derived radiomics features of the cardiac blood pool are associated with cardiac function and motion.

Study Type—Retrospective

Population—26 healthy volunteers (51.2 ± 15.6 years; 17 males)

Field Strength/Sequence—1.5T / balanced steady-state free precession (bSSFP)

Assessment—The radiomics features (107 features in 7 classes) of the blood pool of the left/right ventricle/atrium (LV/RV/LA/RA) were extracted on 4-chamber cine images (25 phases). Conventional cardiac function parameters were assessed in each cardiac chamber (volumes, ejection fraction [EF) and longitudinal strain). Intra- and interobserver agreements of radiomics features of all chambers acquired at all phases were assessed, as well as scan-rescan agreement in a subset of 13 volunteers.

Statistical tests—Pearson correlation coefficients (r) were used to assess the association between peak values of radiomics features and end-diastolic (or maximal) volume, end-systolic (or minimal) volume, EF, and longitudinal strain of corresponding chambers. Good intraobserver, interobserver, and scan-rescan agreements for radiomics features acquired were defined as intraclass correlation coefficient (ICC) > 0.7 or coefficient of variation (CoV) < 20%.

Results—Most radiomics features of the blood pool varied periodically throughout the cardiac cycle. Peak values of chamber-specific blood pool radiomics features were correlated with traditional cardiac function and motion indices of corresponding chambers (r: 0.4 – 0.87). Ninety-three (87%), 86 (80%) and 73 (68%) radiomics features demonstrated good intra-observer, interobserver, and scan-rescan reproducibility, respectively.

Address for correspondence: Kai Lin (kai-lin@northwestern.edu), Department of Radiology Northwestern University 737 N Michigan Avenue, Suite 1600 Chicago, IL 60611, Tel: (312)695-5577, Fax: (312)926-5991.

Conclusion—Cine MRI-derived radiomics features within LV/RV/LA/RA are associated with traditional cardiac function and motion indices of corresponding chambers and may have the potential to become novel quantitative imaging biomarkers in cardiovascular medicine.

Evidence Level—3

Technical Efficacy—1

Keywords

Radiomics feature; Blood pool; Cine MRI

Introduction

Cine MRI is a “standard of care” for measuring cardiac function and motion (1). In addition to the continuous deformation of the myocardium throughout the cardiac cycle, the blood pool signal in the left and right ventricles and atria (LV/RV/LA/RA) also changes with cine phase due to variations in magnetization caused by complex blood flow (or turbulence) (2). Although changes of the blood pool on cine MRI may potentially represent alterations in cardiac function and motion, their diagnostic values have been relatively ignored because such variations in signal intensity or texture on cine images are too tiny to be detected with regular methods and quantified by using common indices, such as the signal-to-noise ratio (SNR) or contrast-to-noise ratio (CNR).

Radiomics refers to a post-processing method for the extraction of pathological characteristics, which are usually undetectable by the “naked eye”, from medical images. By providing rich features that are related to the development and progression of tumors, radiomics has been applied as a “virtual biopsy” to advance diagnosis and therapeutic management in oncology (3). Recently, radiomics analysis has been adopted to evaluate cardiac diseases based on cine MRI (4–6). To date, cardiac radiomics studies have mainly focused on identifying features of the LV wall because the thin walls of the RV/LA/RA make them difficult to delineate (7). However, cardiac diseases can frequently extend beyond the LV wall and they usually manifest as function and motion abnormalities during the course of heartbeats. As a result, the application of radiomics analysis is currently limited in the assessment of cardiac diseases (8).

Describing the variations in the blood pool signal with radiomics analysis seems to be a logical solution to fill these technical gaps in cardiac imaging. Therefore, we extracted radiomics features of the blood pool in the LV, RV, LA, and RA on cine MRI and investigated their correlations with the function and motion patterns of the corresponding chambers in healthy volunteers. The aim of the present study was to test the hypothesis that cine MRI-derived radiomics features of the cardiac blood pool are associated with cardiac function and motion.

Materials and methods

With the approval of the Institutional Review Board (IRB), cine MRI images of 26 healthy volunteers (17 male, mean age: 51.2 ± 15.6 years, range: 27 – 75 years old) were

retrospectively enrolled in the present study. Thirteen of these subjects (9 male, mean age: 52.8 ± 16 years, range: 30 – 75 years old) had two MRI scans within 2 weeks (same imaging protocols and parameters, interval 9 ± 4 days). All participants provided written informed consents before the MRI scans. The inclusion criterion was age: 21 – 89 years old. The exclusion criteria included 1) prior myocardial infarction (MI) or documented coronary heart disease (CHD) or other structural cardiovascular diseases (CVDs); 2) prior coronary artery stenting or prior coronary artery bypass grafting; 3) presence of a permanent pacemaker or cardioverter-defibrillator; 4) atrial fibrillation (AF); 5) claustrophobia, ferromagnetic materials within the body of the patient; 6) excessive abdominal girth preventing entrance into the magnet bore; and 7) inability to lie flat for the MRI scan.

MRI protocol

Cine MRI was performed on a 1.5 T clinical scanner (Magnetom Sola, Siemens Healthcare, Erlangen, Germany) equipped with a 12-channel surface coil (BioMatrix, Siemens Medical Solutions USA, Malvern, PA). A balanced steady-state free precession (bSSFP) cine sequence was acquired in 2-, 3-, 4-chamber, and short-axis views under conditions of breath holding with retrospective ECG gating. Imaging parameters were as follows: repetition time (TR)/echo time (TE) = 3/1.2 ms; acquired temporal resolution 39 ms; flip angle = 65°; voxel size = 2.1 × 2.1 × 6.0 mm^3; gap = 4 mm, bandwidth = 930 Hz/pixel; parallel imaging (GRAPPA technique) with acceleration factor R = 2. Ten to 14 short-axis myocardial slices were acquired to cover the LV/RV from base to apex. Cine acquisitions were reconstructed into 25 phases.

Cardiac motion/function measurements

Images with impaired image quality (defined as signal loss or uncorrected artifacts) were excluded from quantitative analysis. All cine images were transferred to a dedicated image processing workstation (HP, EliteDesk 800 G2 TWR) and analyzed with commercially available software (Circle CVI 42, Calgary, Canada) by reader #1 (KL, with 19 years of experience in cardiac imaging).

After the images were loaded, the artificial intelligence (AI) component of the software automatically detected cardiac landmarks and defined epicardial and endocardial myocardial borders of the LV/RV/LA/RA. The LV/RV volume at each cardiac phase was obtained by summing the LV areas of all slices from the base to the apex of the ventricles. The end-diastolic volume (LVEDV/RVEDV), end-systolic volume (LVESV/RVESV), and ejection fraction (LVEF/RVEF) were then calculated. Maximal and minimal volumes of LA/RA and long axial strains (defined as [change in length]/[original length]) of LV/RV/LA/RA were also calculated.

Radiomics feature extraction

Cine images (4-chamber view) were processed using open-source software (3D Slicer, Version 5.03) (9). The borders of the LV/RV/LA/RA and LV walls on each cardiac phase were manually traced by reader #1. Then, seven classes of original radiomics features of

LV/RV/LA/RA and LV myocardium were extracted by using the Pyradiomics plug-in (10). The features included shape-based (14 features), first-order statistics (18 features), gray level cooccurrence matrix (GLCM, 24 features), gray level dependence matrix (GLDM, 14 features), gray level run length matrix (GLRLM, 16 features), gray level size zone matrix (GLSZM, 16 features), and neighboring gray tone difference matrix (NGTDM, 5 features). Peak values of all radiomic features were obtained from time curves through the entire cardiac cycle. Figure 1 A–C shows the workflow of image processing. Reader #2 performed radiomics analysis independently using the same workflow to test the interobserver variabilities in 13 cases with rescans. Reader #1 reanalyzed these cases a week later to test the intraobserver variabilities.

Statistical analysis

All continuous variables are represented as the mean ± standard deviation (SD). The Pearson correlation coefficient (r) was used to assess the correlations between traditional cardiac indices (EDV, ESV, EF, longitudinal strain) and radiomics features for each chamber. The intraclass correlation coefficient (ICC) and coefficient of variation (CoV, calculated with the root mean square method) were used to assess the intra-, interobserver and scan-rescan agreement of radiomics features (11). One-way ANOVA was used to compare the peak values of radiomics features acquired from the blood pools of different chambers. Statistical analyses were two-tailed and performed using SPSS software (Version 22.0, IBM Corp.). A p value < 0.05 was considered statistically significant. A r value reaching 0.4, 0.6, and 0.8 was considered having a moderate, good, and excellent correlation, respectively. Twenty-six participants will provide a power of 0.9 for detecting a good correlation (assuming $r = 0.6$) between radiomics features and traditional cardiac indices at the level of $\alpha = 0.05$. An ICC value > 0.7 or a CoV $< 20\%$ between repeat measurements was considered to indicate good agreement (12,13).

Results

Cine MRI images of 26 volunteers (and 13 rescans) qualified for analysis. Cardiac function and motion indices were calculated in all subjects. See table 1 for the demographic information and cardiac function and motion indices of the participants.

Time curves showed that most radiomics features of the blood pool varied periodically throughout the cardiac cycle. However, the variation patterns of a single feature in different chambers can be different. There were significant differences in peak values in 69 (64%) features acquired from LV/RV/LA/RA. Figure 2 shows variations in example radiomics features (7 classes; 4 chambers) through the cardiac cycle, averaged over all 26 subjects. Multiple peak values of chamber-specific blood pool radiomics features were correlated with traditional cardiac function and motion indices of corresponding chambers (Table 2).

For the LV blood pool, 21 features were related to the EDV (r: 0.429 – 0.761), 21 features were associated with the ESV (r: 0.421 – 0.804), 1 feature was related to the EF (r = 0.409), and 6 features were associated with the longitudinal strain (r: 0.401 – 0.542). Additionally,

44 of 107 (41%) radiomics features acquired from the LV blood pool were significantly related to their counterparts acquired from the LV myocardium (r: 0.423 – 0.975).

For the RV blood pool, 23 features were related to the EDV (r: 0.414 – 0.717), 26 features were associated with the ESV (r: 0.407 – 0.811), 14 features were related to the EF (r: 0.406 – 0.604), and 16 features were associated with the longitudinal strain (r: 0.412 – 0.615).

For the LA blood pool, 36 features were related to the maximal volume (r: 0.417 – 0.814), 20 features were associated with the minimal volume (r: 0.406 – 0.644), 3 features were related to the EF (r: 0.421 – 0.453), and 4 features were associated with the longitudinal strain (r: 0.402 – 0.489).

For the RA blood pool, 24 features were related to the maximal volume (r: 0.409 – 0.87), 52 features were associated with the minimal volume (r: 0.4 – 0.831), 3 features were related to the EF (r: 0.407 – 0.472), and 16 features were associated with the longitudinal strain (r: 0.404 – 0.545).

Figure 3 shows typical correlations between radiomics features of the blood pool and longitudinal strain of the four chambers.

Ninety-three (87%), 86 (80%), and 73 (68%) radiomics features (using data at all phases) demonstrated good intraobserver, interobserver, and scan-rescan agreement in 13 participants (ICC > 0.7 or CoV < 20%). Figure 4 shows a good scan-rescan reproducibility of “Dependence NonUniformity” (GLDM) in LV/RV/LA/RA.

Discussion

In the current study, we demonstrated distinctive time curves of cine MRI-derived radiomics features of the blood pool in LV, RV, LA, and RA throughout the cardiac cycle. Peak values of these features were frequently correlated to volumes, strain, and EF of corresponding chambers. Additionally, the extraction of most radiomics features of the blood pool is reproducible.

Radiomics is data mining approach for medical images. Recently, radiomics features of the heart and great vessels have been investigated. Kagiyama et al extracted radiomics features from echocardiographic images of 534 patients and found that they can be used to identify myocardial fibrosis (sensitivity 86.4% and specificity 83.3%) (17). In another study of 95 patients with valvular heart disease who were found to have filling defects in the left atrial appendage (LAA) using CT, the receiver operating characteristic curve (ROC) showed that 8 wavelet-transformed features extracted from the filling defects could discriminate 25 cases of thrombus from 70 cases of circulatory stasis with an area under the curve (AUC) of 0.78 (18). Priya et al measured radiomics features on cine images at the mid-LV myocardium of patients with pulmonary hypertension (PH) and controls and, after 45 combinations of feature selection were tested, the AUC reached 0.862 (accuracy: 0.78) in discriminating the two subject groups (19). Neisius et al performed radiomics analysis on native T1 mapping images of 108 patients with hypertrophic cardiomyopathy (HCM) and 53 patients with hypertensive heart disease (HHD). In the final model, 6 radiomics features were able to

efficiently discriminate between HHD and HCM with an overall accuracy of 86.2% and an internally validated accuracy of 80% (20).

However, there are challenges in current radiomics research based on cardiac imaging. First, current cardiac radiomics feature extraction studies have mainly focused on the LV myocardium. As a result, pathologies in other parts of the heart may have been missed. Second, the exact affection of cardiac motion on feature measurements has not been described. In a study with 59 healthy volunteers, Alis et al found that nearly 55% of radiomics features acquired at mid-LV on short-axis cine MRI showed large variability throughout the cardiac cycle (21). This could be a possible reason why only 32% - 47% and 61% - 73% of cine MRI-derived myocardial features were found to be reproducible in inter- and intraobserver analyses, respectively (20). Third, the inclusion of radiomics features lacks a pathophysiological basis to justify its clinical relevance (22). In a study of the UK Biobank, Cetin et al found that certain radiomics features of the LV/LV blood pool and LV myocardium can be used to discriminate participants with traditional cardiovascular risks, such as hypertension, diabetes, high cholesterol, and smoking, from healthy controls (AUC: 0.63 – 0.8) (23). However, selecting radiomics features from a large group of candidates for indicating heart diseases somewhat resembles a computerized “fishing expedition”. Therefore, more reasonable criteria are needed to establish the role of cardiac radiomics features in clinical practice.

The present study was conducted to address these weaknesses of cardiac radiomics analysis. First, we focused on cine MRI-derived radiomics features of the blood pool in LV/RV/LA/RA instead of the LV wall. Radiomics analysis can therefore be applied to evaluate chamber-specific pathology out of the LV area. Second, our data demonstrated variations in radiomics features of the blood pool throughout the cardiac cycle. Therefore, radiomics features can be extracted at distinctive time points within the cardiac cycle to indicate cardiac motion patterns from multiple aspects. Additionally, by including data from all 25 cardiac phases, our study also demonstrated better reproducibility of radiomics features than existing reports (20). Third, multiple physiological or technological mechanisms can be used to explain variations in radiomics features of the blood pool. Levels of some features, such as the “Energy” in the class of “First order”, are prominently confounded by the area (or volume) (24). For a certain chamber, the “energy” level in diastole is usually higher than that in “systole”. Periodical changes in texture features that are roughly independent of the size of the region of interest (ROI), such as “Coarseness” of the “NGTDM”, are thought to result from the signal variations of the blood pool. These can be explained by the physical principles of the bSSFP technique. Generally, the gradient activity of bSSFP is not strictly limited to the slice of the radiofrequency (RF)-excitation (25). The bSSFP signals of the selected slice can be influenced by “out-of-slice” magnetization, from blood flow entering the slice from diverse directions and with different velocities (2). As such, variations in bSSFP-derived radiomics features may indicate intrachamber hemodynamic alterations consequent to cardiac dysfunction. In this sense, radiomics analysis is evolving from a static “virtual biopsy” in oncology to a dynamic “digital catheterization” in cardiac imaging and the application of regular cine MRI has potentially been extended to the domain of hemodynamic assessment (26).

Limitations

First, we did not include patients with existing heart diseases in this study because it is unclear how specific pathological or hemodynamic abnormalities affect radiomics features of the blood pool. To succinctly relate “normal” radiomics features to “normal” cardiac function or motion, we linked peak values of radiomics features to the most commonly used cardiac indices instead of demonstrating numerous correlations between all radiomics features and cardiac indices acquired at the multiple subdivided periods within a cardiac cycle, such as systole, isovolumic relaxation, rapid filling, diastasis and atrial contraction (14). Second, we only extracted radiomics features from the 4-chamber cine because this imaging plane can demonstrate the blood pool of all chambers. Furthermore, because cine MRI is regularly performed under breath holding, acquiring all necessary data from one image plane can avoid the variations caused by inconsistent breath holding during multiple cine imaging acquisitions. Moreover, this choice can shorten the image processing time and simplify the workflow of radiomics extraction. Nonetheless, a study to investigate the consistency of radiomics features acquired from different views of cine MRI is needed in the future. Third, the sample size of this proof-of-concept study is small and there is limited subset reproducibility information. Therefore, we did not evaluate the influences of technical and pathophysiological conditions on radiomics analysis, such as field strength, shim, implant, motion, and flow artifacts. Nonetheless, our promising results showed that future external validation of the blood pool radiomics for the assessment of cardiac health are warranted.

Conclusion

Cine MRI-derived radiomics features within LV/RV/LA/RA are associated with traditional cardiac function and motion indices of corresponding chambers and may have the potential to become novel quantitative imaging biomarkers in cardiovascular medicine.

Funding information and conflict of interest:

This study was supported by grants from the National Institutes of Health (R01HL117888, K01HL121162, R03HL144891).

James Carr has disclosures:

Siemens: research grant to institution; advisory board

Bayer: research grant to institution; advisory board; speaker

Bracco: advisory board

Guerbet: research grant to institution

No other authors have conflict of interest.

References

1. Malayeri AA, Johnson WC, Macedo R, Bathon J, Lima JA, Bluemke DA. Cardiac cine MRI: Quantification of the relationship between fast gradient echo and steady-state free precession

for determination of myocardial mass and volumes. J Magn Reson Imaging 2008;28(1):60–66. [PubMed: 18581356]

2. Scheffler K, Lehnhardt S. Principles and applications of balanced SSFP techniques. Eur Radiol 2003;13(11):2409–2418. [PubMed: 12928954]
3. Shur JD, Doran SJ, Kumar S, et al. Radiomics in Oncology: A Practical Guide. Radiographics 2021;41(6):1717–1732. [PubMed: 34597235]
4. Raisi-Estabragh Z, Izquierdo C, Campello VM, et al. Cardiac magnetic resonance radiomics: basic principles and clinical perspectives. Eur Heart J Cardiovasc Imaging 2020;21(4):349–356. [PubMed: 32142107]
5. Jang J, Ngo LH, Mancio J, et al. Reproducibility of Segmentation-based Myocardial Radiomic Features with Cardiac MRI. Radiol Cardiothorac Imaging 2020;2(3):e190216. [PubMed: 32734275]
6. Jang J, El-Rewaidy H, Ngo LH, et al. Sensitivity of Myocardial Radiomic Features to Imaging Parameters in Cardiac MR Imaging. J Magn Reson Imaging 2021;54(3):787–794. [PubMed: 33650227]
7. Hassani C, Saremi F, Varghese BA, Duddalwar V. Myocardial Radiomics in Cardiac MRI. AJR Am J Roentgenol 2020;214(3):536–545. [PubMed: 31799865]
8. Chang S, Han K, Suh YJ, Choi BW. Quality of science and reporting for radiomics in cardiac magnetic resonance imaging studies: a systematic review. Eur Radiol 2022;32(7):4361–4373. [PubMed: 35230519]
9. Fedorov A, Beichel R, Kalpathy-Cramer J, et al. 3D Slicer as an image computing platform for the Quantitative Imaging Network. Magn Reson Imaging 2012;30(9):1323–1341. [PubMed: 22770690]
10. van Griethuysen JJM, Fedorov A, Parmar C, et al. Computational Radiomics System to Decode the Radiographic Phenotype. Cancer Res 2017;77(21):e104–e107. [PubMed: 29092951]
11. Hyslop NP, White WH. Estimating precision using duplicate measurements. J Air Waste Manag Assoc 2009;59(9):1032–1039. [PubMed: 19785269]
12. Lin K, Sarnari R, Speier P, et al. Pilot Tone-Triggered MRI for Quantitative Assessment of Cardiac Function, Motion, and Structure. Invest Radiol 2022.
13. Koo TK, Li MY. A Guideline of Selecting and Reporting Intraclass Correlation Coefficients for Reliability Research. J Chiropr Med 2016;15(2):155–163. [PubMed: 27330520]
14. Lin K, Sarnari R, Pathrose A, Gordon DZ, Markl M, Carr JC. Cine magnetic resonance imaging detects shorter cardiac rest periods in postcapillary pulmonary hypertension. European heart journal Cardiovascular Imaging 2022.
15. Lin K, Sarnari R, Pathrose A, et al. Cine MRI detects elevated left heart pressure in pulmonary hypertension. J Magn Reson Imaging 2021;54(1):275–283. [PubMed: 33421234]
16. Lin K, Ma H, Sarnari R, et al. Cardiac MRI Reveals Late Diastolic Changes in Left Ventricular Relaxation Patterns During Healthy Aging. J Magn Reson Imaging 2021;53(3):766–774. [PubMed: 33006438]
17. Kagiyama N, Shrestha S, Cho JS, et al. A low-cost texture-based pipeline for predicting myocardial tissue remodeling and fibrosis using cardiac ultrasound. EBioMedicine 2020;54:102726. [PubMed: 32268274]
18. Chun SH, Suh YJ, Han K, et al. Differentiation of left atrial appendage thrombus from circulatory stasis using cardiac CT radiomics in patients with valvular heart disease. Eur Radiol 2021;31(2):1130–1139. [PubMed: 32812175]
19. Priya S, Aggarwal T, Ward C, et al. Radiomics Detection of Pulmonary Hypertension via Texture-Based Assessments of Cardiac MRI: A Machine-Learning Model Comparison-Cardiac MRI Radiomics in Pulmonary Hypertension. J Clin Med 2021;10(9).
20. Neisius U, El-Rewaidy H, Nakamori S, Rodriguez J, Manning WJ, Nezafat R. Radiomic Analysis of Myocardial Native T1 Imaging Discriminates Between Hypertensive Heart Disease and Hypertrophic Cardiomyopathy. JACC Cardiovasc Imaging 2019;12(10):1946–1954. [PubMed: 30660549]
21. Alis D, Yergin M, Asmakutlu O, Topel C, Karaarslan E. The influence of cardiac motion on radiomics features: radiomics features of non-enhanced CMR cine images greatly vary through the cardiac cycle. Eur Radiol 2021;31(5):2706–2715. [PubMed: 33051731]

22. Lambin P, Leijenaar RTH, Deist TM, et al. Radiomics: the bridge between medical imaging and personalized medicine. Nat Rev Clin Oncol 2017;14(12):749–762. [PubMed: 28975929]
23. Cetin I, Raisi-Estabragh Z, Petersen SE, et al. Radiomics Signatures of Cardiovascular Risk Factors in Cardiac MRI: Results From the UK Biobank. Front Cardiovasc Med 2020;7:591368. [PubMed: 33240940]
24. https://pyradiomics.readthedocs.io/en/latest/features.html accessed on 9/15/2022.
25. Miyazaki M, Lee VS. Nonenhanced MR angiography. Radiology 2008;248(1):20–43. [PubMed: 18566168]
26. Abbasian Ardakani A, Bureau NJ, Ciaccio EJ, Acharya UR. Interpretation of radiomics features-A pictorial review. Comput Methods Programs Biomed 2022;215:106609. [PubMed: 34990929]

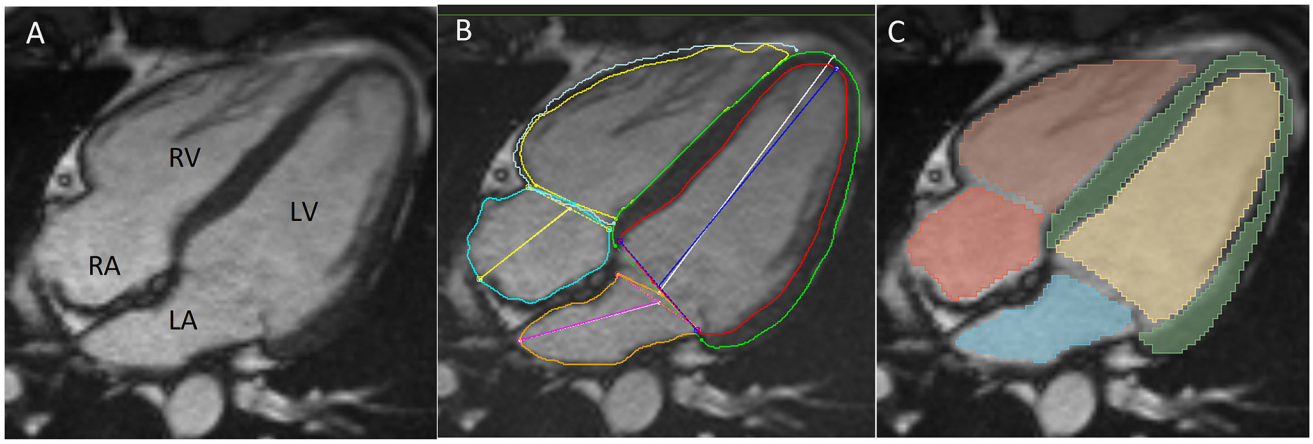

Figure 1.

Cine MRI images were processed to acquire traditional cardiac motion/function indices and radiomics features.

A An original cine MRI image (4-chamber view) at end-diastole

B Acquisition of volumes and longitudinal strains for all chambers with AI function

C Calculation of radiomics features of blood pools and LV myocardium (as a reference for LV blood pool) on the 4-chamber view with manual contour drawing. ROIs are filled with different colors.

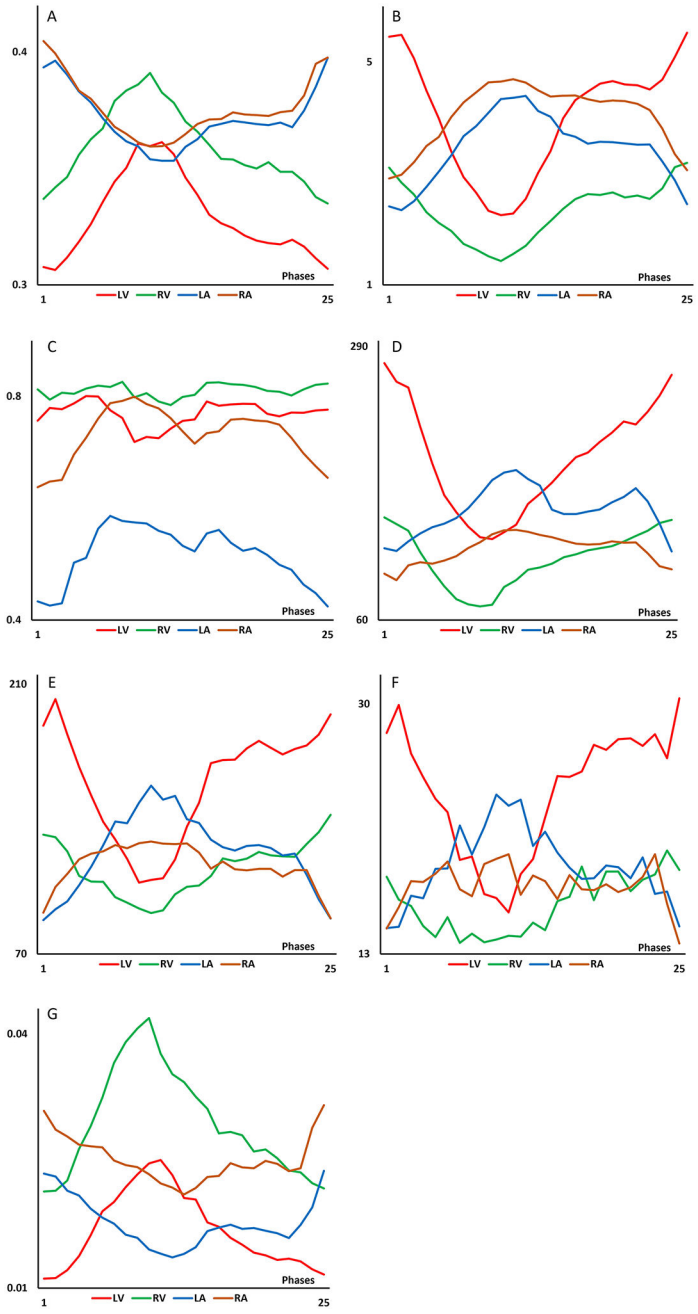

Figure 2.

Variations of 7 typical radiomics features (from 7 different classes) of LV/RV/LA/RA over the cardiac cycle are shown. Trends and peak values of a feature extracted from LV/RV/LA/RA can be significantly different. Radiomics features at each cardiac phase are averaged from the data of 26 participants.

A Sphericity (SHAPE)

B Energy (FIRST ORDER)

C Correlation (GLCM)

D Gray Level NonUniformity (GLDM)

E Run Length Nonuniformity (GLRLM)
F Size Zone Nonuniformity (GLSZM)
G Coarseness (NTGDM)

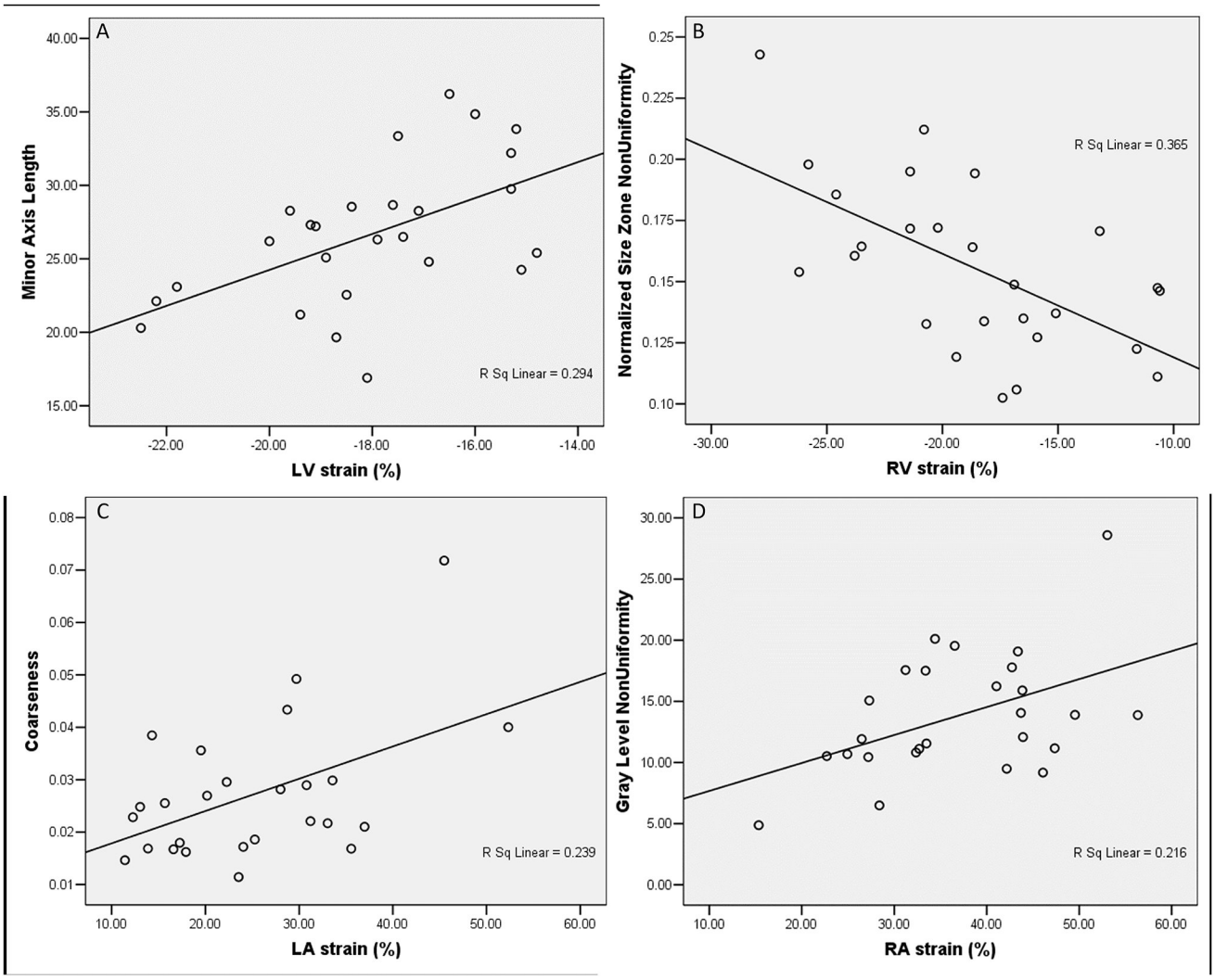

Figure 3.

Scatter plots demonstrate correlations between radiomics features of the blood pool and longitudinal strain of individual chambers ($p < 0.05$).

A The "Minor Axis Length" of the LV (26.7 ± 4.8) is linearly related to LV longitudinal strain ($r = 0.542$).

B The "Normalized Size Zone NonUniformity" of the RV (0.156 ± 0.03) is linearly related to RV longitudinal strain ($r = 0.604$).

C The "Coarseness" of the LA (0.012 ± 0.004) is linearly related to LA longitudinal strain ($r = 0.489$).

D The "Gray Level NonUniformity" of the RA (6.55 ± 2.1) is linearly related to RA longitudinal strain ($r = 0.464$).

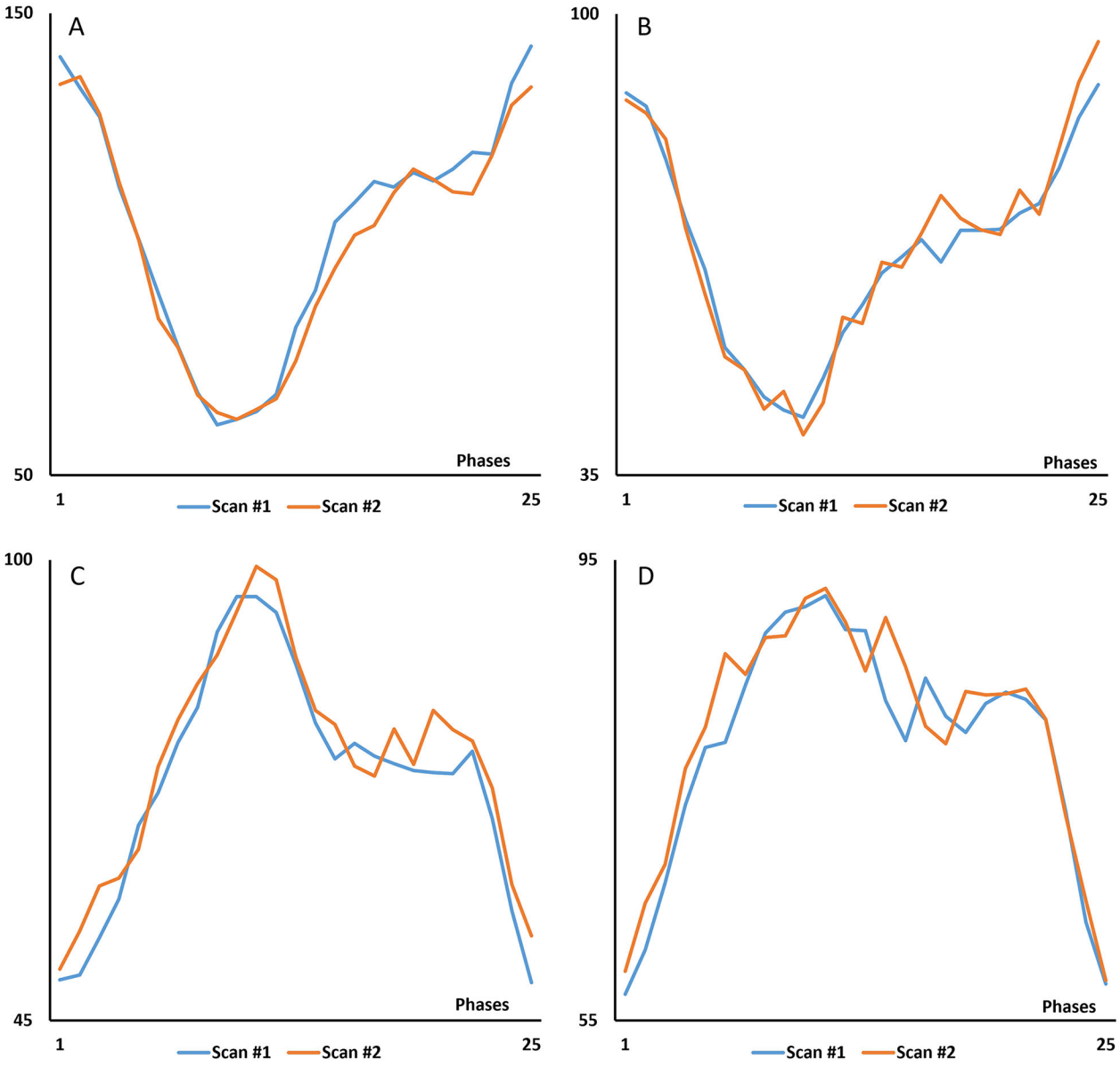

Figure 4.

Time curves demonstrate good scan-rescan reproducibility of "Dependence NonUniformity" (GLDM) through the cardiac cycle. All values are averaged from 13 participants with repeated scans.

A Left ventricle (LV)

B Right ventricle (RV)

C Left atrium (LA)

D Right atrium (RA)

Table 1

Demographic information and cardiac function/motion indices of participants.

Male (%)	17 (65)
Age (years)	51.2 ± 15.6
Height (cm)	172.2 ± 10.2
Weight (kg)	78.1 ± 18
Systolic blood pressure (mmHg)	121.4 ± 17.5
Diastolic blood pressure (mmHg)	73.7 ± 14.8
Heart rate (beats/min)	63 ± 9.2
LVEDV (mL)	148.1 ± 35.1
LVESV (mL)	73.7 ± 14.8
LVEF (%)	56.3 ± 5.5
LV longitudinal strain (%)	−18 ± 2.1
RVEDV (mL)	160.7 ± 41.7
RVESV (mL)	75.2 ± 22.1
RVEF (%)	53.2 ± 6.1
RV longitudinal strain (%)	−18.7 ± 4.8
LA maximal volume (mL)	71.9 ± 16.7
LA minimal volume (mL)	27.1 ± 8
LAEF (%)	62.4 ± 6.7
LA longitudinal strain (%)	25.1 ± 10.3
RA maximal volume (mL)	75.9 ± 26.1
RA minimal volume (mL)	43.2 ± 19.2
RAEF (%)	48.5 ± 6.8
RA longitudinal strain (%)	36.9 ± 9.9

Left ventricle (LV); Right Ventricle (RV); Left atrium (LA), Right atrium (RA); End-systolic volume (ESV); End-diastolic volume (EDV); Ejection Fraction (EF)

Table 2

The number (percentage of total (107) features) of blood pool radiomics features in LV/RV/LA/RA that are related to traditional function/motion indices in individual chambers (defined as $r \geq 0.4$ and $p < 0.05$).

	LV	RV	LA	RA
EDV or maximal volume (%)	21 (20)	23 (21)	36 (34)	24 (22)
ESV or minimal volume (%)	21 (20)	26 (24)	20 (19)	52 (49)
EF (%)	1 (1)	14 (13)	3 (3)	3 (3)
Longitudinal strain (%)	6 (6)	16 (15)	4 (4)	16 (15)